J. Fluid Mech. (1996), vol. 306, pp. 267–292

The effect of free-stream turbulence on sectional lift forces on a circular cylinder

By H. M. BLACKBURN† AND W. H. MELBOURNE

Department of Mechanical Engineering, Monash University, Clayton, Victoria 3168, Australia

(Received 14 November 1994 and in revised form 31 August 1995)

Wind-tunnel experiments were conducted to examine the effect of grid-generated turbulence on lift forces at sections of a circular cylinder. Turbulence of longitudinal intensity between 0.6% and 18% was employed, with cylinder Reynolds numbers in the range 1×10^5 to 5×10^5. Addition of low-intensity turbulence had the primary effect of inducing the critical transition at Reynolds numbers below that for smooth flow; above transition there was little difference between the forces experienced by the cylinder in smooth or turbulent flow, with no sign of organized vortex shedding.

At higher turbulence intensities effects consistent with a return to organized vortex shedding were observed, particularly for the highest intensity and at the upper end of the Reynolds number range; lift coefficients were greater than in smooth supercritical flow, with a broad spectral peak centred near a Strouhal number of 0.23 accompanied by an increase in spanwise correlation lengths of lift force.

1. Introduction

Experimental measurements of lift forces due to vortex shedding downstream of circular cylinders in cross-flow have most often been conducted in smooth flows partly as a consequence of the interest in this fundamental flow. In many applications however, particularly at high Reynolds numbers, the flow fields in which cylinders are immersed are turbulent: for example, in natural flows past large chimney stacks the longitudinal turbulence intensity ($I_u = u'/U$), with U based on the local mean airspeed at a given height, may lie in the range 10% to 20% or greater, while Reynolds numbers usually exceed 1×10^5. It has long been known that the introduction of low-intensity turbulence to the flow field promotes the so-called critical transition at lower Reynolds numbers than is the case in smooth flows, and that increasing the surface roughness of the cylinder has a similar effect (e.g. Fage & Warsap 1930).

The effect of free-stream turbulence and surface roughness at higher Reynolds numbers is less clear, partly due to a lack of experimental data. With smooth cylinders, increasing Reynolds numbers above the critical transition produces (in the nomenclature of Roshko 1961) the supercritical regime, with twin laminar/turbulent separation bubbles, associated narrow wake and low force coefficients, followed by a gradual transition to the transcritical regime, associated with fully turbulent boundary layer separation and somewhat higher force coefficients. Since both the cylinder boundary layer and the wake will be fully turbulent, it is expected that after

† Current address: CSIRO, Division of Building, Construction and Engineering, PO Box 56, Highett, Victoria 3190, Australia.

the transcritical regime is reached there will be no further transitions, with the flow and force coefficients becoming independent of Reynolds number. In the transcritical regime, experimental data (James, Paris & Malcolm 1980; Shih *et al.* 1993) and boundary-layer models (Güven, Patel & Farell 1977) suggest that increased cylinder surface roughness induces transition to transcritical flows at lower Reynolds numbers and produces larger force coefficients.

The effect of turbulence on flows in the transcritical Reynolds regime has received little systematic study, but data from a small number of full-scale experiments suggest that free-stream turbulence may also produce higher force coefficients in the transcritical regime (Vickery & Daly 1984). This effect can be partially attributed to low-frequency cross-flow buffeting by free-stream turbulence; however examination of lift spectra suggest that another, as yet unknown, mechanism also serves to increase lift force spectral density at the Strouhal frequency in the transcritical regime. The influence of turbulence in the supercritical to transcritical transition is uncertain, although it has been suggested by Zdravkovich (1991) that sufficiently high levels of turbulence would effectively obliterate the supercritical regime by disrupting the formation of laminar/turbulent separation bubbles, with transition to the transcritical regime occurring directly from the subcritical. Previous wind-tunnel studies (So & Savkar 1981; Cheung & Melbourne 1983; West & Apelt 1993), conducted with Reynolds numbers near and above 1×10^5, show that introduction of free-stream turbulence acted to increase cylinder lift coefficients above those for smooth supercritical flow, but do not completely characterize the nature of the flows; for example, lift autospectra and spanwise correlations of lift were not presented. In addition, turbulence intensities were moderate, with maximum longitudinal intensities of 7.5% in the study of West & Apelt and 9.1% in that of Cheung & Melbourne. In the experiments of So & Savkar and Cheung & Melbourne, the forces measured were those acting on a finite length of cylinder, rather than at a cylinder section, and no attempt was made to correct the results for a lack of spanwise correlation of lift. West & Apelt employed a number of pressure transducers located on one cylinder diameter in order to better characterize sectional lift forces.

In this paper we describe a series of wind-tunnel experiments conducted using a fixed circular cylinder equipped with six sectional lift force transducers in which the Reynolds number of the mean flow was varied in the range 1×10^5 to 5×10^5. Since lift forces were measured simultaneously at six locations along the span of the cylinder, information about the spanwise organization of lift could be extracted in addition to information about sectional forces. A turbulence-generating screen could be inserted upstream of the cylinder to provide longitudinal intensities up to 18%, well into the range experienced in full scale. The longitudinal integral scale of the turbulence was approximately one-half the cylinder diameter. Results are presented for standard deviation of coefficient of lift C_l', lift autospectra S_{C_l} and dimensionless spanwise correlation length of lift force, Λ. The data strongly suggest that the introduction of high-intensity turbulence acted to promote a return to comparatively strong but broadband vortex shedding.

2. Equipment

The experiments were conducted using the Monash University 450 kW boundary-layer wind tunnel, which is equipped with a variable-pitch axial-flow fan so that a range of air speeds may be achieved. With a 2 m high by 1 m wide working section installed, the maximum air speed in smooth flow was 55 m s^{-1}, reducing to 45 m s^{-1}

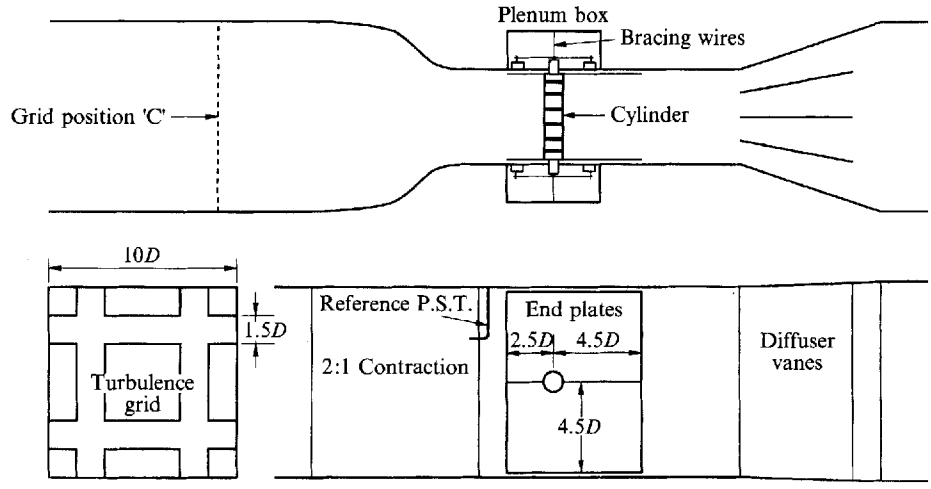

FIGURE 1. 2 m × 1 m working section of Monash University 450 kW wind tunnel, showing dimensions of end plates, turbulence screen and location of screen in position C (closest to the cylinder).

with the turbulence screen in place. A plan view and elevation of the working section are shown in figure 1. An end elevation shows the dimensions of the turbulence screen, which was placed in the 2 m by 2 m section, upstream of the contraction. The screen was made from four flat sheets of wood. It could be installed in three positions, at distances 47.5D, 29.5D and 18D upstream from the cylinder centreline (position A, B and C respectively; position C, the closest to the cylinder, is indicated in figure 1). Just upstream of position A, wire screens and aluminium honeycomb were permanently installed to reduce the turbulence levels in nominally smooth flow.

End plates were mounted 50 mm from the working section walls in order to isolate the cylinder from the wind-tunnel wall boundary layers, which were of the order of 50 mm thick at the cylinder position. End-plate boundary-layer depth at the cylinder centreline position was 0.1D in the smooth flow. The end plates extended 9D cross-flow, 2.5D upstream and 4.5D downstream of the cylinder centreline, after the recommendations of Stansby (1974). Small gaps between the ends of the cylinder and the end plates were sealed with synthetic fur.

A reference Pitot-static tube was installed upstream of the cylinder and displaced in the cross-flow direction to reduce interference with flow past the cylinder. Corrections between the Pitot-static tube readings and mean flow velocities at the cylinder centreline position were obtained from measurements made using hot-film probes with the cylinder removed from the working section. Thus the Pitot-static tube readings were calibrated to give the mean velocities in turbulent flow.

The cylinder had a diameter of 200 mm and a length of 900 mm, producing an aspect ratio of 4.5:1 and a tunnel blockage of 10% in the cross-flow direction. The moderate values of aspect ratio and blockage were chosen as compromises between conflicting objectives of high Reynolds number, high aspect ratio and low blockage.

The cylinder was assembled from six transducer segments and seven 'blanks', all mounted on a structural aluminium tube of smaller diameter, as shown in figure 2. The transducer segments were narrow (0.1D) in the axial direction, with the aim of providing good estimates of sectional lift forces. Axial spacing of the transducers was 0.75D. The transducer outer sections were mounted from the inner structural tube on

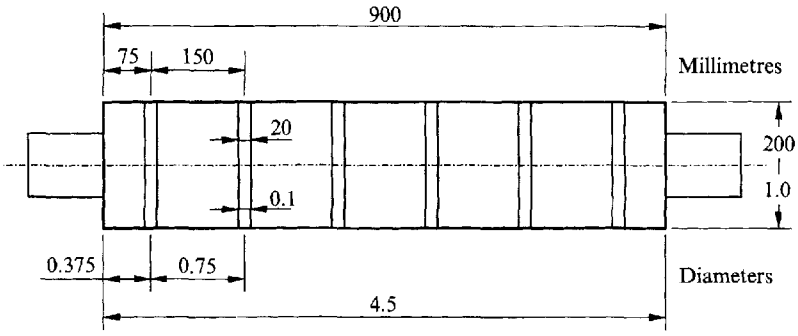

FIGURE 2. Cylinder assembly showing locations and dimensions of the six lift force transducers. An internal structural cylinder is responsible for the reduced-diameter protrusions at cylinder ends.

metal beam springs to which semiconductor strain gauges were bonded in a full bridge configuration that minimized response to moments and drag forces. The resonant frequency of the transducer segments on the beam springs was approximately 400 Hz.

Measurements of the cylinder assembly showed that the maximum variation in radius at any section was 0.2 mm or 0.1% D, while the standard deviation of cylinder diameter along the axis was 0.12 mm. All segments were painted with epoxy and rubbed back to a smooth, glossy finish. Transducer and 'blank' segments were separated by 0.5 mm gaps which were covered with 30 μm polyurethane film elastomer, glued in place.

Along the rear generator of the cylinder, 18 pressure tappings were installed, with reference pressure provided by the the static pressure line of the reference Pitot-static probe. Pressures were computed from readings obtained using an inclined tube manometer bank.

During tunnel running, measurements were taken simultaneously at the six lift force transducers by digitizing and storing the outputs of transducer strain bridge amplifiers. Each recording consisted of 8192 × 6 samples obtained at a frequency of 400 Hz, giving a Nyquist frequency of 200 Hz. Prior to sampling, transducer signals were passed through a set of analogue low-pass filters to remove components above 150 Hz. A Perkin-Elmer 3210 minicomputer was used for data collection, back-up to magnetic tape, and subsequent off-line signal processing.

For additional detail concerning cylinder construction, transducer calibration and signal processing, consult Blackburn (1992), Blackburn & Melbourne (1992).

3. Flow field

Four flow configurations were chosen to provide three turbulence intensities in addition to the nominally smooth flow obtained with no screen. Turbulent fluctuations in the longitudinal and cross-flow directions were measured with X-configuration hot-film sensors at the cylinder axis position. Results are presented in terms of streamwise and cross-flow turbulence intensities (standard deviation divided by mean value) $I_u = u'/U$ and $I_v = v'/U$ in figure 3. Spanwise-averaged values of these quantities are provided in table 1, together with estimates of the turbulence longitudinal integral scale ratio L_u^x/D, obtained by fitting von Kármán spectra of the form

$$\frac{\Upsilon S_u(\Upsilon)}{u'^2} = \frac{4\Upsilon L_u^x}{\left[1 + 70.8(\Upsilon L_u^x)^2\right]^{5/6}} \tag{3.1}$$

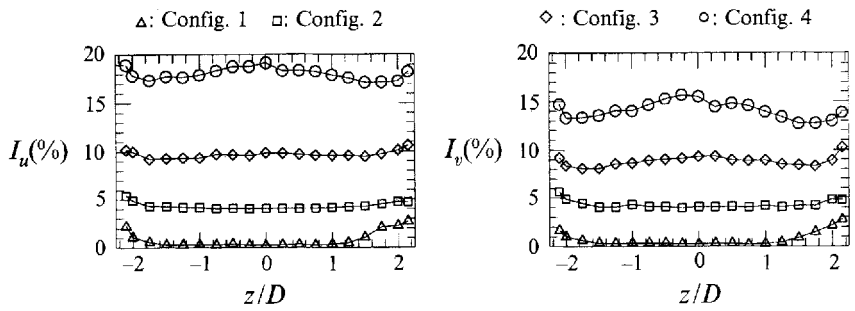

FIGURE 3. Distributions of longitudinal and transverse turbulence intensities ($I_u = u'/U$ and $I_v = v'/U$) along cylinder axis position for the four flow configurations.

Configuration	Description		I_u%	I_v%	L_u^x/D
1†	Wire screens;	position A	0.6	0.6	0.10
2	Turbulence screen;	position A	4.2	4.2	0.50
3	Turbulence screen;	position B	9.6	8.7	0.53
4	Turbulence screen;	position C	18.0	14.1	0.53

† 'Smooth flow'

TABLE 1. Spanwise-averaged turbulence intensities and the ratios of turbulence integral scales to diameter for the four flow configurations.

to longitudinal turbulence spectra ($\Upsilon = f/U$ is the inverse wavelength of the fluctuations under Taylor's hypothesis).

Mean flow velocities were measured at the cylinder axis position with a hot-film probe; the mean velocities were within 2% of the spanwise-averaged values for all flow configurations.

It can be seen in table 1 and figure 3 that as turbulence intensity increased the average values of streamwise and cross-flow intensity diverged and the spanwise distributions became less uniform. This fact alone indicates departure from isotropy at high intensities which is largely a consequence of the relative proximity of the turbulence screen to the cylinder position at high turbulence intensities. The screen had been made comparatively coarse (see figure 1) in an attempt to provide the largest practicable integral scale and at position C the cylinder centreline was three mesh spacings downstream of the screen ($x/M = 3$). Batchelor (1953) cites a streamwise distance of $x/M = 10$ for ratios of streamwise and cross-flow grid turbulence intensities to become independent of streamwise direction. In addition, the 2:1 contraction would have introduced some further anisotropy in all the turbulence configurations, tending to increase the ratio of cross-flow to streamwise intensities (Uberoi 1956). Despite these departures from homogeneous, isotropic conditions, the results for the highest turbulence intensity are felt to be important enough to justify their inclusion here. The deviation from ideal conditions is an inevitable consequence of using turbulence screens to generate high-intensity turbulence. In full-scale applications, high turbulence intensities typically occur in boundary-layer flows which are neither homogeneous or isotropic.

4. Results

4.1. *Introductory remarks*

Results concerning averaged values of sectional lift coefficients and sectional lift force autospectra will be described in §4.2. Relationships between forces measured at different cylinder sections will be covered in §4.3.

No correction for tunnel blockage or cylinder aspect ratio has been applied to the results as a consequence of uncertainty about the validity of correction measures over the range of Reynolds numbers obtained in this experiment. We defer further discussion of these effects until §5. Lift coefficients and Reynolds numbers have been calculated using free-stream velocities obtained using readings from the reference Pitot-static tube and corrected to cylinder centre-position values.

As described in §2, lift force measurements were obtained using transducers with an axial length of $0.1D$. While this can be regarded as significant in relation to some of the observed spanwise correlation lengths ($1D$ minimum), the results are described here as sectional measurements for ease of reference. Under reasonable assumptions, the theoretical difference between true sectional values of standard deviation of lift coefficient, C_l', and those found using the very short transducers employed in this experiment is small, of order 1% (see e.g. Blackburn 1994).

Lift spectra have been obtained from time series recorded at one transducer location, typically one of the two central locations, and are given in dimensionless form, normalized such that the area of the spectrum equals the variance of coefficient of lift, and with a dimensionless frequency $f_r = fD/U$, i.e.

$$\int_0^\infty S_{C_l}(f_r)\,\mathrm{d}f_r = C_l'^2. \tag{4.1}$$

Spectral estimates were prepared using the method of overlapping segment-averaged periodograms with a raised-cosine data window (Press *et al.* 1992, §13.4), while mean values were removed from each segment prior to Fourier transformation. Values were obtained at 257 frequencies over the range 0–200 Hz, giving a 0.781 Hz increment between successive estimates, while thirty estimates were averaged at each frequency point; owing to the variation in mean flow speed with Reynolds number the reduced frequency increment changed with Reynolds number, with a range of approximately $0.0208 < f_r < 0.00417$ over $1 \times 10^5 < Re < 5 \times 10^5$. For the method of overlapping periodograms, the standard deviation of the spectral estimate at any frequency point is approximately $[11/(9K)]^{1/2}$ times the expected value, where K is the number of overlapping averages (see Press *et al.*); this gives a standard deviation of approximately 20% of the expected value for $K = 30$, which accounts for the 'noisy' appearance of many of the experimentally derived spectra of lift presented below.

4.2. *Characteristics of sectional lift*

Values of C_l' are shown as functions of Reynolds number for all flow configurations in figure 4; the effects of increases in turbulence intensity in first promoting the transition to the critical regime and then producing higher levels of C_l' are immediately apparent. The values presented in figure 4 and the remainder of the paper are the averages of the values of C_l' obtained at the four transducers nearest the centreline of the tunnel, with the aim of providing representative values upon which the discussion of the effects of Reynolds number and turbulence intensity can be based.

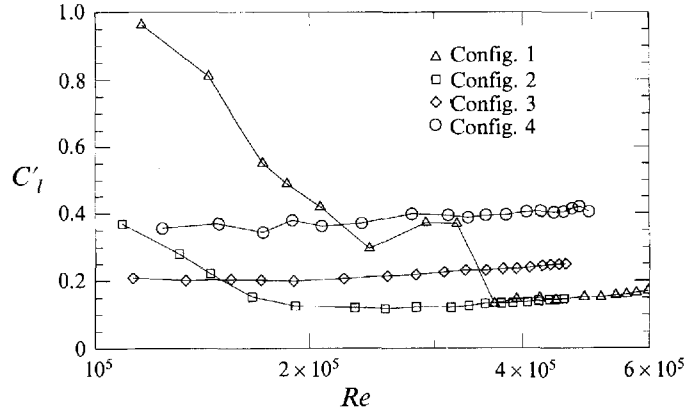

FIGURE 4. Standard deviations of lift coefficient as functions of Reynolds number for all four flow configurations. Values are the averages of C'_l taken over the four most central transducers.

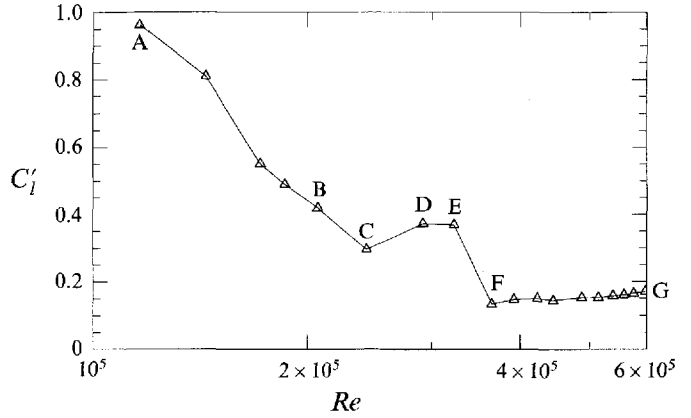

FIGURE 5. Standard deviations of sectional lift coefficient as functions of Reynolds number for smooth flow ($I_u = 0.6\%$). Values are the averages of coefficients from the four most central transducers. A: $Re = 1.16 \times 10^5$, B: $Re = 2.07 \times 10^5$, C: $Re = 2.43 \times 10^5$, D: $Re = 2.92 \times 10^5$, E: $Re = 3.23 \times 10^5$, F: $Re = 3.65 \times 10^5$, G: $Re = 5.99 \times 10^5$.

4.2.1. *Flow configuration 1, smooth flow, $I_u = 0.6\%$*

The values of C'_l for smooth flow are repeated in figure 5, with points of reference labelled A–G. C'_l at first dropped as Re increased, progressing from $C'_l = 0.96$ at $Re = 1.16 \times 10^5$ (point A) to 0.42 at $Re = 2.07 \times 10^5$ (point B). This regime has been called the precritical by Zdravkovich (1991).

As C'_l fell with increasing Re in the initial regime (A–B), the Strouhal number remained relatively constant near 0.2. Gaussian-bell-shaped curves were fitted to the lift spectra, as proposed by Vickery & Clark (1972), allowing $S_{C_l}(f_r)$ to be parameterized in terms of the Strouhal number St, variance of coefficient of lift C'^2_l, and a dimensionless bandwidth B:

$$S_{C_l}(f_r) = \frac{C'^2_l}{\pi^{1/2} B\, St} \exp\left[-\left(\frac{f_r - St}{B\, St}\right)^2\right]. \tag{4.2}$$

The outcomes of this curve fitting are presented in figure 6; they show that the major change was a drop in C'_l, with an accompanying slight reduction in spectral

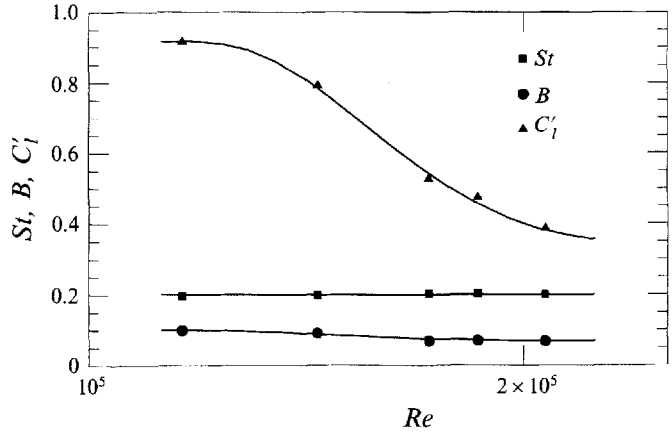

FIGURE 6. The spectral parameters Strouhal number (St), bandwidth (B) and standard deviation of coefficient of lift (C_l') fitted to the lift forces measured in smooth flow. Values are averages from the two central transducers.

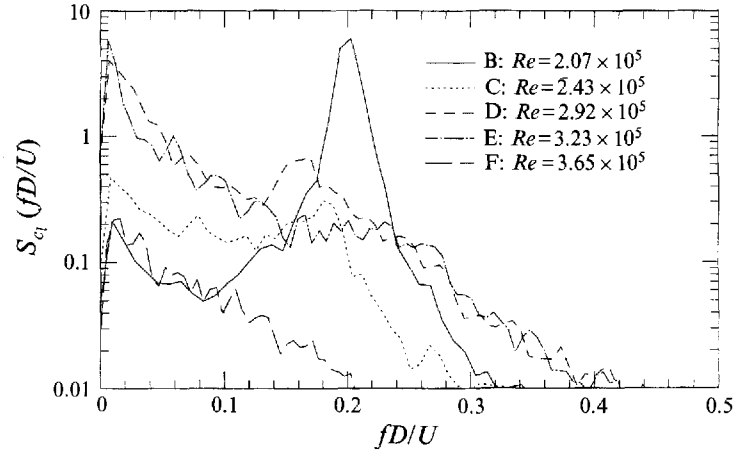

FIGURE 7. Smooth flow: changes in lift spectra during the transition B–F.

bandwidth B (although this latter effect can in part be attributed to reduced bias errors brought about by lower f_r increments at higher Reynolds numbers). It will be shown in § 4.3 that the spanwise correlation of lift remained relatively constant in this regime, despite the drop in C_l'.

The initial fall in values of C_l' as Reynolds numbers increased was followed by a slight rise in C_l' at $Re = 2.92 \times 10^5$ (D) and 3.23×10^5 (E), before C_l' dropped again at $Re = 3.65 \times 10^5$ (F) to reach an approximately constant value over the rest of the Reynolds number range. Lift spectra for the transition B–F are shown in figure 7.

Figure 7 shows that the collapse of the spectral peak at $f_r = 0.2$ was accompanied by an increase in low-frequency energy. In the spectra for both C and E there are indications of weak spectral peaks at reduced frequencies 0.18 and 0.16 respectively, but at the higher Reynolds number of point E there was no sign of such a peak, with the lift spectral density falling monotonically from the lowest frequency point. The large rise in low-frequency energy for points D and E was reflected in the unsteadiness of the lift forces; in particular, the time series for point D indicated

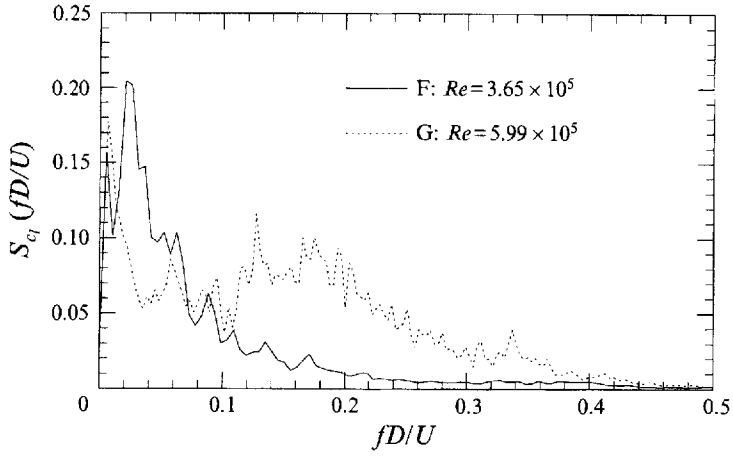

FIGURE 8. Spectra of lift force at points corresponding to F and G in figure 5.

occasional bursts of comparatively well-organized vortex shedding interposed between large low-frequency fluctuations.

At the end of this transition C_l' fell by nearly two-thirds, from 0.37 (at point E) to 0.13 at point F. The corresponding spectra in figure 7 reveal similar distributions of lift spectral density over reduced frequency, but with a much reduced level for F. Note that at point F (and over the remainder of the *Re* range) there was no evidence of the high-frequency vortex shedding ($St \approx 0.48$) that has been reported by some other investigators in this regime (Bearman 1969; Achenbach & Heinecke 1981; Schewe 1983): this issue is taken up again in § 5.2. For the remainder of the Reynolds number range (up to 5.99×10^5), values of C_l' increased to 0.17, and there was a gradual evolution of spectral shape, eventually showing a very broad hump in the lift spectrum, centred near $f_r = 0.16$, in addition to low-frequency energy. This point is illustrated in figure 8.

4.2.2. *Flow configuration 2, $I_u = 4.2\%$*

This was the first of the three flow configurations in which turbulence was deliberately introduced to the flow.

At the low end of the Reynolds number range, where values of C_l' dropped as *Re* increased, lift spectra showed broad peaks with Strouhal numbers of approximately 0.18, while the bandwidth and 'background noise' were greater than for the smooth subcritical flow. A spectrum recorded at $Re \approx 1.1 \times 10^5$ is presented in figure 9. At the high end of the Reynolds number range, the values of C_l' were similar to, but slightly higher than, those found for smooth flow. The similarity was reflected in the lift spectra, with spectral densities which decreased monotonically with frequency (figure 10). At the high end of the Reynolds number range, lift spectra at all spanwise locations had a similar shape, showing a monotonic decline in spectral density with increasing frequency.

In general, the results at the high end of the Reynolds number range for configuration 2 were similar to those obtained in the smooth flow; the increase in turbulence intensity had little effect other than providing a slight increase in variance of coefficient of lift.

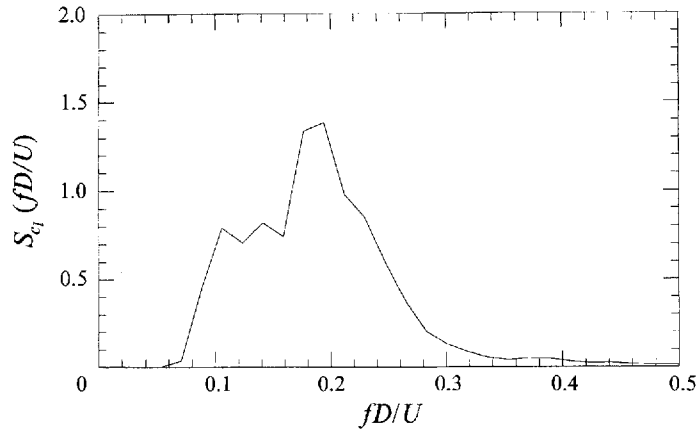

FIGURE 9. Spectrum of lift near the lower end of the Reynolds number range for flow config. 2 ($I_u = 4.2\%$), $Re \approx 1.1 \times 10^5$.

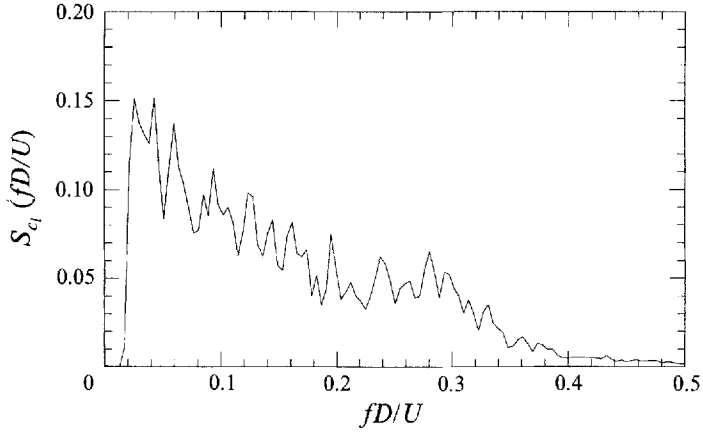

FIGURE 10. Spectrum of lift near the upper end of the Reynolds number range for turbulence config. 2. (Compare figure 8 G.) $Re = 5.37 \times 10^5$.

4.2.3. *Flow configuration 3, $I_u = 9.6\%$*

Figure 4 shows that introduction of turbulence of 9.6% intensity produced a large increase in lift coefficients at the high end of the Reynolds number range when compared with results for lower levels of turbulence. In addition, the figure shows that there was less variation in C_l' with Re over the range investigated, indicating that the critical transition (if this can be said to occur for flows with high turbulence intensities) took place at Reynolds numbers below those which could be measured in the experiments. The upward trend of C_l' with Re (from 0.21 at $Re = 1.13 \times 10^5$ to 0.25 at $Re = 4.59 \times 10^5$) shows that complete Reynolds number independence was not achieved.

The distribution of C_l' along the span was not completely uniform, and became less so with increased Reynolds number. This trend was reflected in the lift force spectra, which showed variation in shape along the span, particularly at the higher Reynolds numbers. Figure 11 shows the spectra from the six force transducers at $Re = 4.59 \times 10^5$. While the spectra for the end-most transducers had densities which dropped monotonically with frequency, those recorded at the centre of the cylinder

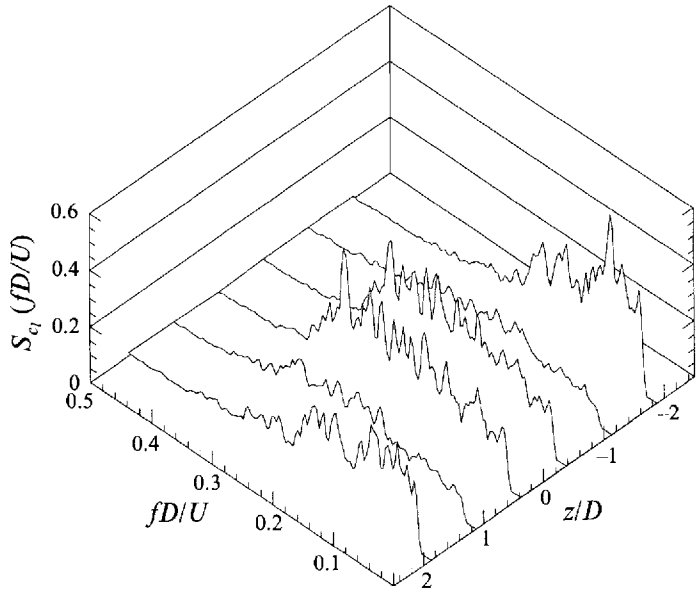

FIGURE 11. Turbulence config. 3: spectra of lift force from all six transducers at $Re = 4.59 \times 10^5$.

displayed a broad plateau of lift spectral density up to $f_r \sim 0.35$. Note that the shapes of the spectra at the ends of the cylinder were similar to those for configuration 2 (figure 10).

The variation in shape of the spectra along the span and the fact that at the centre of the span and at high Reynolds numbers the spectral density did not decrease monotonically with frequency suggests that the increases in C_l' above those found at the lower turbulence levels are not just due to increased buffeting by the lateral components of incident turbulence. If the increased lift were due to quasi-steady buffeting alone, it would be expected that the spectra of lift would decrease monotonically with frequency from low frequencies, as that is the shape of the turbulence spectra.

4.2.4. *Flow configuration 4, $I_u = 18\%$*

A further increase in turbulence intensity to 18% brought about higher values of C_l' across the Reynolds number range than did the the two lower intensity configurations, as shown in figure 4. Values of C_l' rose from 0.36 at $Re = 1.24 \times 10^5$ to 0.41 at $Re = 4.95 \times 10^5$. Some caution should be applied when interpreting these results, however, since as was pointed out in § 3, the turbulence screen was quite close to the model position for this flow configuration.

Apart from the increase in values of C_l' brought about by increased turbulence intensity, the most striking feature of this set of results when compared to the lower turbulence configurations was the reappearance of dominant peaks in the lift force spectra, centred at a Strouhal number of approximately 0.23. It is thought that this dominant peak reflects re-establishment of organized vortex shedding. An example spectrum, recorded at the upper end of the Reynolds number range ($Re = 4.95 \times 10^5$) is shown in figure 12.

It is apparent that besides there being a definite peak near $f_r = 0.23$, the spectrum was broad, and there was considerable energy down to low frequencies (the fact that there is no energy at the very lowest frequencies in figure 12 reflects digital

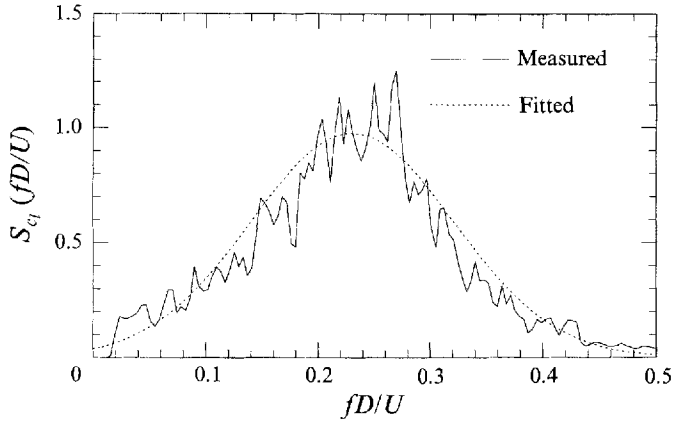

FIGURE 12. Turbulence config. 4: spectrum of lift force recorded at one of the central transducers at $Re = 4.95 \times 10^5$. Also shown for comparison is a fitted spectrum of the form given by equation (4.2). Measured value of $C_l' = 0.46$; fitted value 0.47.

high-pass filtering carried out during data processing). The broadness of the spectra makes it difficult to make definite conclusions as to the partition of lift energy into components due to vortex shedding and cross-flow buffeting by the lateral components of turbulence, a point which will be taken up again in § 5.

As noted above, C_l' rose by about 12% as Reynolds numbers increased through the range. This rise was accompanied by a slow evolution in spectral shape. To illustrate this effect, spectra of the form (4.2) were fitted to the measured spectra using least-squares techniques, as was done for the smooth flow data. An example of a fitted curve is shown in figure 12, in which it can be seen that the fitted Gaussian bell folds into the negative frequency range. This means that the fitted values of C_l' to be presented are overestimates, and must be regarded as indicative of trends rather than exact (refer to figure 4 for measured values). The results of the curve fitting procedure are shown in figure 13 (compare figure 6 for smooth subcritical flow) where the values shown are the average of those for the two most central transducers. The rise in the measured values of C_l' with Re was reflected in the fitted results, while the plot also reveals that the Strouhal number remained relatively constant near 0.23 over the range, and that the bandwidth B of the spectra gradually decreased. Note that the values of spectral bandwidth ($B \sim 0.6$) were much greater than those for smooth subcritical flow ($B \sim 0.07$).

The spanwise distribution of C_l' became less uniform as turbulence intensity increased from 9.6% to 18%. This was true over the entire range of Re for configuration 4, while non-uniformity increased with Re for configuration 3 from almost uniform values at the lowest end of the Reynolds number range. While the general trend of an increase of C_l' towards the centre of the span for configuration 4 may be linked to the same trend at the upper end of the Reynolds number range in configuration 3, it may well be a consequence of increased turbulence intensity near the centre of the span for configuration 4 as described in § 3.

4.3. *Spanwise relationships*

Since measurements of lift force were obtained simultaneously with six lift force transducers, it is possible to present information about the instantaneous and statistical relationships between lift occurring at different spanwise locations. As noted in § 2,

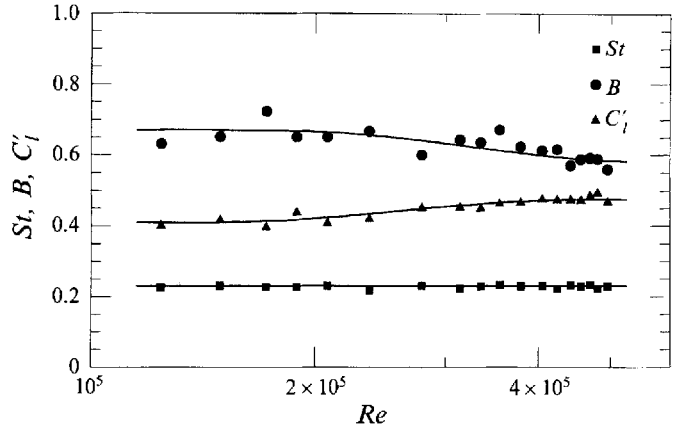

FIGURE 13. Turbulence config. 4: Parameters for fitted sectional coefficient of lift spectra. Values are averages of those obtained from the two most central transducers.

the transducers were mounted at axial spacings of $0.75D$, distributed symmetrically about the tunnel centreline.

4.3.1. *Lift/time series surfaces*

It was found that for the smooth subcritical flows, the length scales of spanwise variation of lift were large in comparison to transducer spacing. This made feasible the interpolation along the span of time series from the six transducers to form smooth surfaces of lift/time series. In the computations of the surfaces, processed time series (each 8192×6 points) were split into smaller blocks of 500×6 points, so that events of the order of one vortex-shedding cycle in duration could be more readily identified.

Many features of the lift process are readily seen by viewing these surfaces, as illustrated by the example presented in figure 14. In the figure, two views of the same section of surface are presented: in figure 14(*a*), the viewpoint is directly above the surface, central along the cylinder span and midway through the section of time series, while in figure 14(*b*) the viewpoint is again centrally located in time but displaced along the spanwise direction. In figure 14(*a*), the four horizontal lines of discontinuity represent the time series from the four transducers centrally located on the cylinder; the time series from the outer two lie on the edges of the box (the discontinuities are an artefact of the simulated lighting of the surface).

A number of interesting features may be seen in figure 14. For most of the time represented, lift, and hence vortex shedding, was comparatively well-organized along the span. At approximately the middle of the record, the phase maintenance of shedding along the span broke down, with vortex shedding drifting out of phase to the extent that lift could be positive at one end of the cylinder and negative at the other – a phase difference of π. Despite the phase drift, the shedding was apparently well-organized in other ways: for example, the vortices extended over the entire span of the cylinder without interruption, and the phase variation was linear along the span. When the lift at the ends of the cylinder was opposed in phase (approximately sixteen vortex shedding periods from the start of the record), a 'vortex dislocation' occurred, with the evolution of an 'extra vortex' on one end of the cylinder. This production can more easily be seen figure 14(*b*): 30 peaks can be counted on the lift force trace at the side of the box furthest from the viewer, with 31 on the closer side.

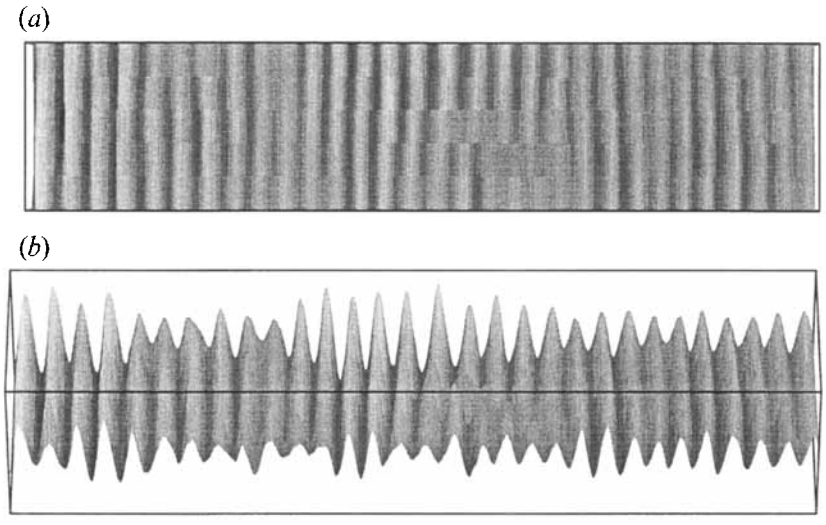

FIGURE 14. Visualized lift/time series surface for smooth subcritical flow ($Re = 1.6 \times 10^5$). Approximately 30 vortex-shedding cycles are represented. (*a*) View from above the surface (spanwise direction: up and down page; time coordinate: across page; coefficient of lift: normal to page). (*b*) Same surface, but with the viewpoint displaced in the spanwise direction.

After the dislocation, the spanwise organization of vortex shedding was disrupted for a short time (2–3 periods) until strong spanwise organization was re-established with shedding in phase along the cylinder.

At Reynolds numbers above the critical transition in smooth flow, and for the turbulent flows, the spanwise length scales of lift force became smaller in relation to the spacing of transducers (as will be discussed below), so that the lift/time series surfaces became less easy to interpret.

4.3.2. *Lift cross-correlation*

As illustrated in figure 14, the forces at the separate transducers bore some similarity to one another. A full spectral description of the statistical relationship between the forces at the various stations would have required a 6×6 matrix of lift force cross-spectra for each data set; in order to reduce the description to more readily comprehended proportions a simplified approach has been adopted. A conventional simplification used in design calculations is to compute the cross-correlation coefficient between the forces at different spanwise locations

$$\rho_{z_1 z_2} = \left(\overline{C_{l_1} C_{l_2}} - \overline{C_{l_1}}\ \overline{C_{l_2}}\right) / C'_{l_1} C'_{l_2}, \tag{4.3}$$

and to then approximate the real parts of the cross-spectra of lift at different stations by the correlation coefficient multiplied by the square-root of the products of the autospectra at each station. This is reasonable if the out-of-phase components of the cross-spectra are small (or not important in applications) and the cross-correlation is not a function of frequency, i.e. the cross-correlation measured over a band of frequencies is constant over the frequency spectrum. It was found that both these conditions were closely satisfied by the experimental data, as has also been found by other investigators (e.g. Surry 1972).

The correlation coefficients between the forces at the six transducers in each set of data can be represented as symmetric 6×6 matrices; the symmetry is a consequence of the definition of cross-correlation. If the vortex shedding process

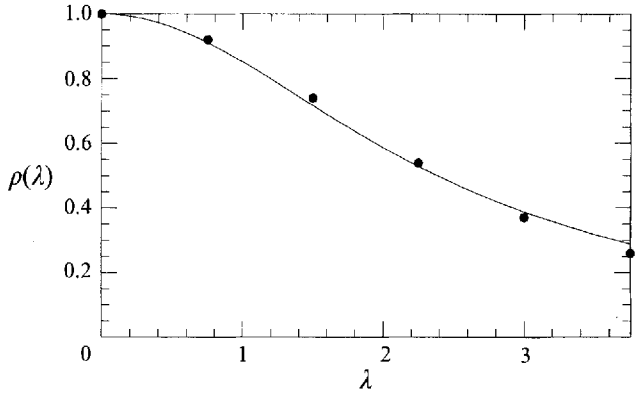

FIGURE 15. Spanwise distribution of the average correlation coefficient of lift force. Also shown is a fitted curve which provides a correlation length Λ of $\sim 3.75D$.

were spanwise-homogeneous, then the matrix elements along diagonals parallel to the leading diagonal would be expected to be equal also. In order to further condense the information, average values of the correlation coefficient were computed for one, two, three, four and five transducer spacings by taking the average values on the diagonals successively removed from the leading diagonal. A set of example average correlation coefficients obtained in this way is plotted in figure 15. One graph of this type was produced from each data recording.

All the results were found to have distributions of a similar shape, and it was decided that for the purpose of extrapolation they could be represented reasonably well by one-parameter curves of the form

$$\rho(\lambda) = \left[1 + \left(\frac{\pi}{2\Lambda}\right)^2 \lambda^2\right]^{-1}, \tag{4.4}$$

in which $\lambda = |z_1 - z_2|/D$ is the dimensionless spanwise spacing at which the average correlation coefficient is evaluated. It is easy to verify that the dimensionless correlation length

$$\Lambda = \int_0^\infty \rho(\lambda)\, \mathrm{d}\lambda. \tag{4.5}$$

By fitting curves of the form (4.4) to diagonally averaged values of $\rho(\lambda)$, as shown in figure 15, the correlation matrix computed for each set of results could be represented by one number, Λ. Dimensionless correlation lengths fitted in this manner are presented for each flow configuration as functions of Reynolds number in figure 16. It can be seen that the spanwise correlation in smooth flow remained relatively high, near $3.75D$, until the onset of critical transition at $Re = 2.43 \times 10^5$ (point C in figure 5), when the correlation length dropped to reach values near $1.25D$. In turbulent flow, the correlation length had values between $1.0D$ and $1.25D$ over most of the Reynolds number range for configurations 2 and 3. In the highest intensity turbulence, configuration 4, the correlation length increased to a value of $1.5D$ over the entire Reynolds range. It is thought that this is related to the re-establishment of dominant peaks in the lift force spectra, and indicates a return to comparatively well-organized vortex shedding. It is possible that the relative proximity and coarseness of the turbulence screen could have influenced the correlation results in configuration 4;

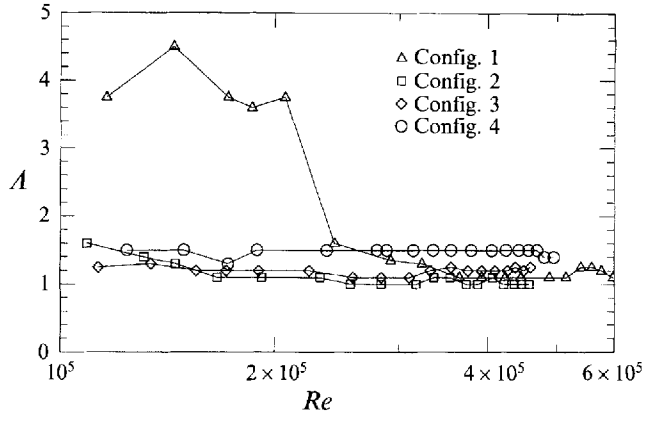

FIGURE 16. Dimensionless correlation lengths of lift forces as functions of Re for the four flow configurations used.

however the turbulence integral length scale ($\sim 0.5D$) is smaller than the observed lift correlation length ($\sim 1.5D$).

5. Discussion

5.1. *Preliminary*

A number of general points need to be made as a preface to the discussion.

The first concerns the comparison of measurements of lift force between experiments in which the lengths of transducers are different proportions of cylinder diameter. Since vortex-induced forces are not perfectly correlated along the span except at Reynolds numbers below approximately 180, it is obvious that a fluctuating coefficient of lift obtained with a short transducer will be greater than that obtained with a long transducer, other things equal. On the basis of analysis described by Blackburn (1994) and the observed spanwise correlation lengths of lift force, it is thought that the short ($0.1D$) transducers used in the present work would offer good estimates of the sectional forces.

The next point concerns the effects produced by the combination of cylinder and working section geometry. In ideal circumstances, one would wish to have measurements of lift obtained from sectional transducers on an infinitely long cylinder in a flow of infinite extent; in practice, it is known that the proximity of working section walls affects the flow. There are three main aspects which are to some extent interconnected: cylinder end conditions, cylinder aspect ratio (ratio of length to diameter) and tunnel blockage (ratio of cylinder diameter to tunnel cross-flow dimension).

Since free cylinder ends produce a large influence on the flow for many diameters along the cylinder axis, tests are usually made with cylinder ends butted to tunnel walls or large end plates; geometrically there should be no difference between the two provided the extent of the plates is sufficiently large in relation to cylinder diameter. The difference must come from the different ratios of wall boundary-layer depth to cylinder diameter (this ratio is reduced by the use of end plates); in turn, this will influence the size of the 'necklace' or 'horseshoe' vortical structures at the junction of the cylinder and the wall. The depth of the end-plate boundary layers is minimized by keeping the upstream extent of the plates comparatively short ($O(2D)$); however a

compromise must be made so that the plates do not become so short that the end flows are not effectively constrained by the plates. The cross-flow and downstream extents of the plates are made as large as possible; again the minimum size is determined by the requirement that the end plates effectively constrain the cylinder-wall flow. The size of the end plates in the present experiment was in accordance with the experimental results of Stansby (1974, see also § 2).

The use of properly designed end plates can serve only to reduce rather than eliminate end effects, since the 'necklace' vortices must still interact with vortex shedding and in addition the presence of an end wall/plate must act to locally constrain three-dimensional wake flow. In results for the subcritical flow regime published by Fox & West (1990), end effects were observed in measurements of base pressure for a distance of approximately 3.5D from the end plates, producing a maximum decrease in C_{pb} next to the plates of approximately 5%; near the centre of the span, measurements of C_{pb} were unaffected provided the end plates were at least 7D apart. Measurements of C_l' (obtained using circumferentially distributed pressure taps at the tunnel centreline) were approximately 7% higher when the end plates were 5D apart than when the end plates were 10D, 15D or 25D apart. These results are in accord with measurements published by Keefe in 1962, and similar results have recently been published by Szepessy & Bearman (1992).

There is some difficulty in considering the influence of end effects and aspect ratio separately, since a decrease in aspect ratio obviously brings the ends of a cylinder closer together. The experimental results of Keefe, Fox & West and Szepessy & Bearman support the view that the main effect of decreasing the aspect ratio is to increase the proportion of the cylinder over which end effects are felt, although according to Szepessy & Bearman the degree of sensitivity is Reynolds number dependent. Before turning to discuss effects of tunnel blockage, we will record here one of the observations made by Achenbach & Heinecke (1981) concerning the effects of aspect ratio on Strouhal numbers in the supercritical regime (Reynolds numbers just above the critical transition). They found that at the same blockage ratio, high-frequency shedding ($St \approx 0.5$) was observed in the wake of a smooth cylinder of aspect ratio 6.75:1, while no Strouhal peak could be found in measurements for a cylinder of aspect ratio 3.38:1.

Tunnel blockage effects are caused by the constraint which tunnel walls parallel to the cylinder axis give the flow past any object inserted in the tunnel, so that streamlines (pressure distributions etc.) are distorted from what they would be if the object were placed in an infinite flow. The effects of blockage on flows past circular cylinders are complex, mainly as a result of the fact that the separation point is free to take up any position on the cylinder. By constraining the wake flow, blockage first influences the separation point by changing the pressure gradients on the body. Secondly, the increase in local velocity at the boundary of the cylinder brought about by the constraint can have an effect similar to that of increasing the Reynolds number, which also influences where separation occurs. A further consideration is that the constraint imposed by blockage may well affect the nature of three-dimensional wake features, as indicated by the results of Blackburn (1994).

These difficulties make it impossible to reliably apply the various theoretical and semi-empirical blockage correction procedures suggested in the past, even in sub-critical flows (see West & Apelt 1982); it would seem that in the Reynolds number regime near the critical transition only a systematic experimental study could determine the appropriate blockage corrections. In the absence of such a study, no blockage correction has been applied to the experimental results reported here; how-

ever it is known that the general effect of increased blockage in the subcritical regime is to increase all the force coefficients, both mean and fluctuating. The results of Richter & Naudascher (1976) show this clearly, but although they were careful to change only the blockage and not the aspect ratio (8.6:1) of their cylinder, the fluctuating lift values they reported were measurements of C_l' obtained using an active cylinder length of $6D$; in the absence of accompanying measurements of the effect of blockage on spanwise correlation it was not considered advisable to use their results to correct sectional values of C_l' obtained in this experiment.

Taken as a whole, the above considerations imply that measurements of sectional lift in the present experiment, obtained with a cylinder of 10% blockage ratio and an aspect ratio of 4.5:1, are likely to be higher than those obtained in an unblocked flow and with a higher aspect ratio. Comparisons with other experimental results, to be discussed below, confirm this expectation: for example, in smooth subcritical flow, where many other experimental results are available for comparison, the indications are that the measurements obtained here are higher than those for low-blockage, high-aspect-ratio flows by a factor in the range one and a half to two. The situation is less clear at higher Reynolds numbers and in turbulence. No results are yet available which show the effects of blockage in the supercritical and transcritical regimes; however it may be expected that any increases in force coefficients would be smaller than in subcritical flows since the width of the wake and hence the constraint applied by the tunnel walls will be smaller. The effects of variations in cylinder aspect ratio should also be less noticeable in highly turbulent, high Reynolds number flows than in smooth subcritical flows owing to the apparently reduced correlation lengths of wake structures, and hence of lift, in turbulence. Consequently one would expect the differences between the sectional lift coefficients presented here and those that would be obtained on a section of an infinite cylinder in an unconstrained flow to be smaller for the turbulent flows than for smooth subcritical flow.

Owing in part to a lack of comparable wind-tunnel results, some observations of C_l' made in full-scale natural flows past reinforced concrete structures are reviewed in the following discussion of turbulent flow results. The justification for including these results is that they were obtained at high Reynolds numbers and in highly turbulent flows. The full-scale measurements of sectional coefficients of lift would be expected to be somewhat different to those obtained here, owing to the different influence of free-end effects, higher surface roughnesses, taper, and higher Reynolds numbers in the full-scale flows. However, perhaps the most significant difference between the full-scale flow regimes and those in the present experiments lies in the ratio of integral scale of turbulence to cylinder diameter. In the experiments, $L_u^x/D \approx 0.5$, but the ratio was of order 10 for the full-scale results. The likely consequences of this will be discussed below.

The main theme of the results is that a return to organized vortex shedding at supercritical Reynolds numbers was apparently promoted by the introduction of turbulence to the mean flow, an effect that is likely to be independent of details of tunnel blockage, cylinder aspect ratio or turbulence scale.

5.2. *Smooth flow*, $I_u = 0.6\%$

The measurements conducted at the lower Reynolds numbers ($Re < 2.07 \times 10^5$) indicate that the flow was precritical, on the basis that the values of C_l' fell with increased Reynolds number while the Strouhal number remained relatively constant near 0.2 (figure 6). An interesting feature of the measurements was that the spanwise correlation length remained relatively constant in this regime ($\Lambda \approx 3.75$, see figure 16).

Experiment	Date	Measured	L_{active}/D	L_{cyl}/D	Blockage(%)	I_u(%)
Present Study		Force	0.1	4.5	10	0.6
Gerrard	1961	Pressure	—	6.7 (min) ¶	15 (max) ‡	0.3
Jones *et al.*	1969	Force	2.33	5.3	18.6†	0.17
Batham	1973	Pressure	—	6.7	5	0.5
So & Savkar	1981	Force	3.0	8	16	0.5
Schewe	1983	Force	10.0	10	10†	0.4
Cheung	1983	Force	6.7 (max)	3.6 (min) ¶	15 (max) ‡	0.4
Norberg & Sundén	1987	Pressure	—	8.83	9.6	1.4
West & Apelt	1993	Pressure	—	> 10	6, 10	0.2

† Slotted tunnel walls; ‡ Blockage corrected; ¶ A number of different cylinders.

TABLE 2. Experimental details for published measurements of lift made in nominally smooth flows, together with those from this experimental programme. L_{cyl}/D is the cylinder aspect ratio, while L_{active}/D is the transducer aspect ratio.

This suggests that the drop in force coefficients often observed in this regime is a result of essentially two-dimensional effects (such as a lengthening of the vortex formation region) in agreement with the assessment of Zdravkovich (1991).

Other experimental studies provide a basis for comparison of the values of C_l' obtained in smooth flow: graphical and tabular summaries of other measurements are provided in table 2 and figure 17, with the results from this experimental programme included for comparison. The smooth-flow results lie in the high end of the scatter band in subcritical flow and above the majority of other published results in the supercritical regime, although in both regimes our results are comparable with those published by So & Savkar (1981). Some of the published experimental values for C_l' would naturally be somewhat lower than those presented here, since in many of the experiments lift forces were measured on substantial lengths of cylinder, rather than on the comparatively short lengths used here. The discrepancy would be larger in supercritical flows, where the spanwise correlation scales of lift forces are lower (see results of Bruun & Davies 1975). Those considerations aside, it is expected that the values obtained here in subcritical flow would be somewhat high, on the basis of the moderate values of tunnel blockage and cylinder aspect ratio, as discussed in § 5.1. In subcritical flow, the results of West & Apelt (1993) are thought to provide accurate estimates of the sectional values of C_l', since much care was taken to obtain good estimates of true sectional lift coefficients and to avoid the influences of aspect ratio and tunnel blockage. West & Apelt's measurements are similar to those of Fox & West (1990) and Keefe (1962), also obtained with high cylinder aspect ratios and low tunnel blockages (for clarity, these two additional sets of results are not shown on figure 17).

The brief rise in values of C_l' in smooth flow at the start of the critical regime (points D & E in figure 5) was noted in § 4.2. The spectral results and observations of the time series indicate that the rise in C_l' was due to intermittent bouts of vortex shedding interspersed with low-frequency lift fluctuations, with energy near the precritical Strouhal number and at low frequencies both contributing to the rise in C_l'. This behaviour suggests intermittent formation of single laminar–turbulent

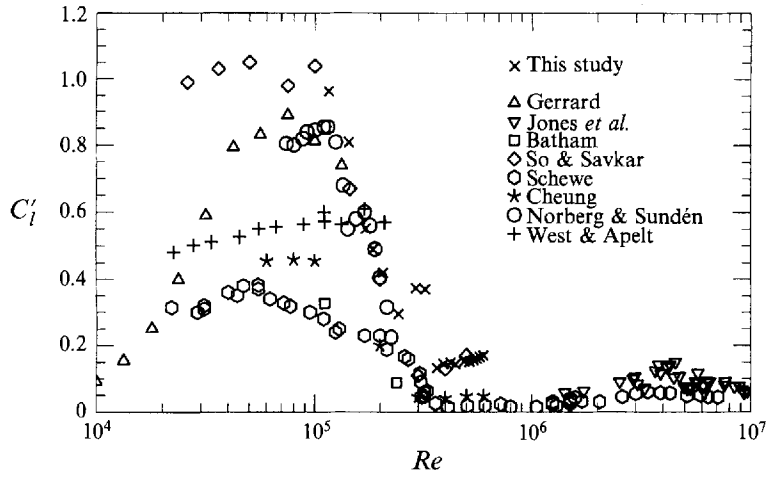

FIGURE 17. Published measurements of C_l' for nominally smooth flows, compared with those from this experimental programme.

separation bubbles, on one side of the cylinder at a time. Similar behaviour was observed in the transition range of Reynolds number by Farell & Blessman (1983).

In the supercritical regime, the high values of C_l' may be partly due to the fact that this set of experimental results was obtained from measurements of force on short sections of cylinder, while the other published results (Jones, Cincotta & Walker 1969; So & Savkar 1981; Cheung 1983; Schewe 1983) were obtained by measuring forces on significant lengths of cylinder (see table 2). The results of So & Savkar are coincidentally in close agreement with ours, which probably indicates that their results were artificially high as a result of high tunnel blockage (their 16% blockage is the highest of the fully enclosed working sections). Compensation for spanwise correlation could be attempted; however spanwise correlation effects alone cannot account for the differences between the various sets of results since the nature of the flow differed between experiments: for example, Schewe found organized vortex shedding in the supercritical regime, with a Strouhal number of 0.48, while in the remaining experiments listed in table 2 (including the present one), the spectra of lift forces were broad, with no dominant Strouhal peaks. As reported by Achenbach & Heinecke (1981), this difference may be due to differences in cylinder aspect ratio; the aspect ratio of Schewe's cylinder (10:1) was higher than those in the other experiments. Bearman (1969), employing a hot-wire anemometer in the wake of a 12:1 aspect ratio cylinder, also observed a Strouhal number of 0.48.

5.3. *Turbulent flows*

The influence of turbulence on lift force spectra is summarized in figure 18, where spectra recorded at one transducer at the upper end of the Reynolds number range for each of the flow configurations are compared.

A comparison of values of C_l' measured in this programme of tests with those published by other workers for this Reynolds number range is presented in figure 19. Turbulence parameters for the various experiments are summarized in table 3; other physical details were presented in table 2. It may be seen that values of L_u^x/D were similar for all the results in table 3.

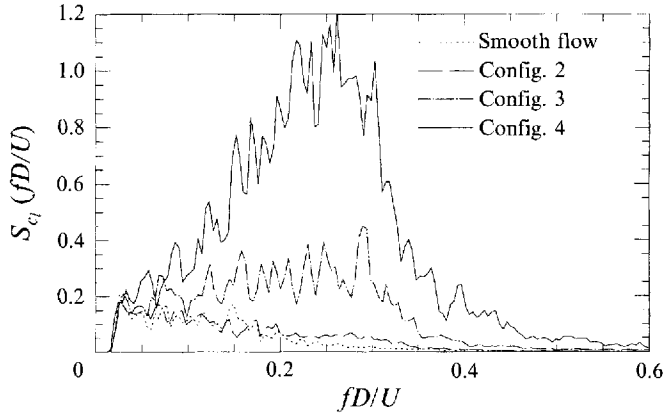

FIGURE 18. A comparison of lift force spectra recorded at transducer 4 at Reynolds numbers near 4.6×10^5 in smooth and turbulent flows.

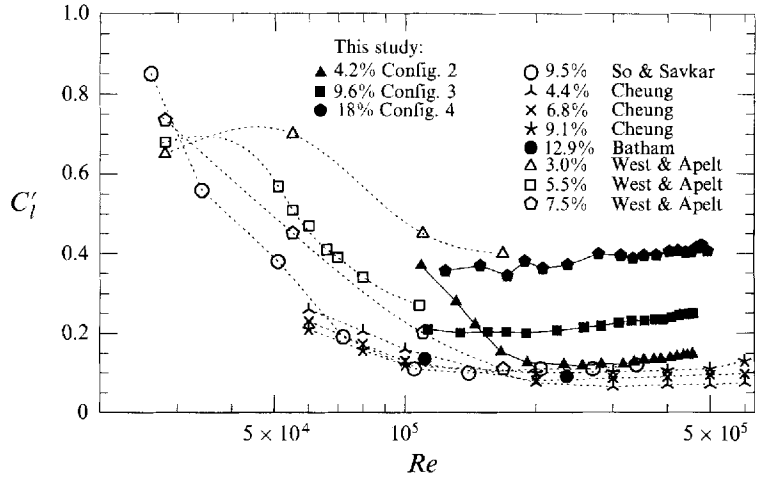

FIGURE 19. Values of C_l' for turbulent flow compared with those found by Batham (1973), So & Savkar (1981), Cheung (1983) and West & Apelt (1993).

5.3.1. *Flow configuration 2, $I_u = 4.2\%$*

At the low end of the Reynolds number range, the gradual loss of organized vortex shedding, coupled with a reduction in lift coefficient, shows that the critical transition was induced at lower Reynolds number than in smooth flow, but was spread over a wider band of Reynolds number. The reduction in C_l' was accompanied by a slight drop in correlation length, but this was not as large a drop as for the smooth-flow case. Once the supercritical regime was reached, lift spectra and coefficients of lift were very similar to those obtained in the nominally smooth flow, indicating that at these Reynolds numbers the primary effect of the comparatively low-intensity turbulence was to promote early transition to supercritical flow.

In figure 19, the results of Cheung (1983), for $I_u = 4.4\%$, may be compared with these measurements. Cheung's results are lower than those presented here, which is partly attributable to the effects of low spanwise correlation (since he measured lift forces on the entire cylinder) and partly to his blockage correction, which had greater effect at low Reynolds numbers where the discrepancy is greatest.

Experiment	Date	$I_u(\%)$	L_u^x/D
Present Study		4.2–18.0	0.5
Batham	1973	12.9	0.5
So & Savkar	1981	9.5	0.8
Cheung	1983	4.4–9.1	0.5
West & Apelt	1993	3.0–7.5	0.5

TABLE 3. Experimental details for published measurements of lift made in grid turbulence, together with those from this experimental programme. Values of L_u^x/D are approximate.

The two lowest turbulence intensities of West & Apelt (1993) quoted here, 3.0% and 5.5%, bracket the intensity used in our experiment, 4.2%. Their tests only extended into the lower range of Reynolds numbers employed here; however, in the region of overlap, West & Apelt's sectional values of C_l' lie to either side of those presented here. Since the tunnel blockage for those results of West & Apelt included here was 9.5%, similar to the 10% blockage in the present sets of results, while their cylinder aspect ratio was higher, the apparent agreement between the two sets of results encourages the view that cylinder aspect ratio effects may be less significant in highly turbulent flows than in smooth subcritical flows.

5.3.2. *Flow configuration 3, $I_u = 9.6\%$*

By comparison with the results for the lower turbulence intensities, the spectra of lift force for flow configuration 3 showed evidence of the return of a broad peak, with reduced low-frequency energy at the highest Reynolds numbers (figures 11 and 18).

The results of Batham (1973, $I_u = 12.9\%$), So & Savkar (1981, $I_u = 9.5\%$), Cheung (1983, $I_u = 9.1\%$) and West & Apelt (1993, $I_u = 7.5\%$) may be compared with those presented here for configuration 3 ($I_u = 9.6\%$). The results from this experimental programme were larger than those of the other experiments on the whole, except for the sectional measurements of West & Apelt, where there is reasonable agreement in the regime where the Reynolds numbers overlap.

The results of Batham, So & Savkar, and Cheung are similar, which is perhaps unexpected, since the results of Batham, obtained from fluctuating pressure measurements at one section of the cylinder, should be higher than the other two sets if the values of C_l' were uniform along the spans of the cylinders used and if other factors were the same. In fact, reference to table 2 shows that Batham's results were obtained with a blockage ratio of 5%, lower than that employed by either Cheung or So & Savkar. A possibility is that competing effects caused by lower blockage and sectional lift force measurements in Batham's case cancelled out to provide the similarity between the three sets of results.

5.3.3. *Flow configuration 4, $I_u = 18\%$*

The effect of increasing the turbulence intensity to 18% was to increase the values of C_l' and A, together with the establishment of a clear (but broad) spectral peak in lift forces, centred near $St = 0.23$. In addition, the spanwise correlation of vortex shedding increased in this configuration above that observed at high Reynolds numbers for the other flows (see figure 16). Taken together, these effects suggest that high-intensity turbulence may act to produce transcritical flows with associated vortex shedding at Strouhal numbers near 0.2 at lower Reynolds numbers than in smooth flows, as proposed for example by Zdravkovich (1991). The reader should bear in mind,

however, the caveats issued earlier concerning screen-proximity effects on the incident turbulence. The effects of tunnel blockage and cylinder aspect ratio should also be taken into consideration, although as argued above, these effects are probably less significant in influencing vortex shedding in highly turbulent than in smooth flows.

The gradual increase in C_l' and decrease in B with Reynolds number (see figure 13) indicate that Reynolds number independence was not fully established at the highest Reynolds numbers in the experiment. Despite this, the prospect of Reynolds number independence in flows of Reynolds numbers which are low compared to those experienced in full-scale makes a comparison with available full-scale data obtained in turbulent flow particularly interesting, even with the provisos mentioned above concerning data from full-scale measurements taken into consideration.

5.3.4. *Full-scale results*

Ruscheweyh & Hirsch (1975) gave values of C_l' and lift force spectra obtained from pressure measurements on the Hamburg television tower, a tapered reinforced concrete structure 275 m high (measurements were obtained at an elevation of 78.8 m). The surface roughness of the structure was quoted as $3.7 \times 10^{-4} D$ which although not large is almost certainly large enough to have influenced the results: typically an increase in surface roughness produces increased force coefficients in the transcritical regime. At $Re = 6.7 \times 10^6$, a value of $C_l' = 0.18$ was obtained in a flow with $I_u = 15\%$ and it has been estimated that L_u^x/D was of the order of 10 for this flow. Analysis of their lift force spectrum revealed a distinct spectral peak at $St = 0.20$, with a bandwidth parameter $B \approx 0.38$. There was substantial, but not dominant, energy at low-frequencies, due to the buffeting effects of turbulence.

Sanada & Nakamura (1983) and Sanada, Suzuki & Matsumoto (1992) published results measured on a 200 m high reinforced concrete stack; the readings were obtained from pressure tappings installed at an elevation of 140 m where the diameter was 15 m. The results have also been reproduced and discussed by Vickery & Daly (1984) and Vickery (1991). The surface roughness for this structure is not known, but is likely to be comparable to that for the Hamburg television tower. Narrow-band vortex shedding ($St = 0.21$) was reported, again with substantial low frequency energy due to incident turbulence contributing approximately 25% of the overall fluctuating lift. Over the range of Reynolds numbers from 1×10^7 to 4×10^7, C_l' dropped from approximately 0.4 to 0.07. Vickery & Daly (1984) and Vickery (1991) suggested that this drop could was correlated not with increase in Reynolds number but with a decrease in turbulence intensity, as assessed from the ratio $C_d'/\overline{C_d}$. Since a large proportion of the overall lift was due to vortex shedding as opposed to buffeting, it was suggested that turbulent energy in the mean flow was able to enhance the forces produced by vortex shedding.

On the basis that it is most likely to be the fine scales of turbulence (scales less than some fraction of the cylinder diameter) that interact with the vortex shedding processes, Vickery proposed that a generalized Taylor parameter of the form $Ta = I_u \left(L_u^x/D\right)^{-1/3}$ be used as a correlating parameter for sectional lift forces in turbulent flows, reflecting both the energy of incident turbulence and that proportion of it which resides at wavelengths small compared to cylinder diameter. In figure 20, estimates made by Vickery & Daly of Ta and C_l' from a number of full-scale measurements obtained at high Reynolds numbers (primarily those of Sanada & Nakamura) are presented, showing that there does appear to be a trend for C_l' to increase with Ta. Values obtained in the current experiments at the upper end of the Reynolds number range ($Re \approx 5 \times 10^5$) for flow configurations 3 and 4 are also plotted on figure 20.

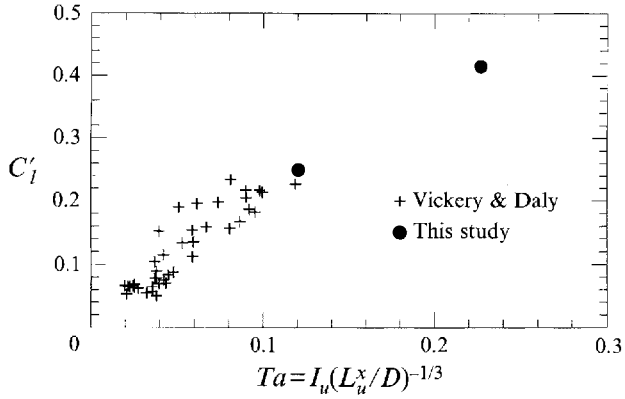

FIGURE 20. Estimates of sectional coefficients of lift C_l' and turbulence parameter $Ta = I_u \left(L_u^x/D\right)^{-1/3}$ presented by Vickery & Daly (1984), together with values obtained at the upper end of the Reynolds number range ($Re \approx 5 \times 10^5$) in the present experiments.

It can be seen that these two experimental values extend the range of the turbulence parameter Ta above the full-scale results, and that the values of C_l' follow the trend established by the full-scale results.

The mechanism by which fine-scale turbulence could act to enhance lift forces is uncertain, but it may cause a thickening of the cylinder boundary layer, leading to earlier separation and consequent higher forces. It is known that increasing cylinder surface roughness (hence, thickening the boundary layer) has the effect of reducing separation angle and increasing mean drag coefficients in the transcritical regime (Shih *et al.* 1993).

6. Conclusions

6.1. *Smooth flow*

In the precritical regime, C_l' dropped with increasing Reynolds number, but the Strouhal number remained constant at 0.20. The spanwise correlation length remained nearly constant, $A \approx 3.75$, up to the onset of the critical transition, indicating that the changes in force coefficients in the precritical regime are due to two-, rather than three-dimensional effects. The nature of these two-dimensional effects remains to be investigated; possibly they are associated with a lengthening of the vortex formation region rather than a movement of separation points, since the Strouhal number remained nearly constant.

In the precritical regime, the values of C_l' were high by comparison to values obtained by most previous investigators; this is thought to be due to the use of a cylinder with moderate tunnel blockage and aspect ratio. In the supercritical regime, no definite Strouhal peak was observed and the spanwise correlation length of fluctuating lift forces was approximately one cylinder diameter. Again, it is thought that the absence of high-frequency vortex shedding in the supercritical regime could be attributed to the use of a comparatively low cylinder aspect ratio.

6.2. *Turbulent flow*

Results obtained for the flow with $I_u = 4.2\%$, $L_u^x/D = 0.50$ indicated that the turbulence acted mainly to promote early transition to supercritical flow, and the

results obtained at the upper end of the Reynolds number range were very similar to those obtained in the nominally smooth flow.

The results for the two highest turbulence intensities ($I_u = 9.6\%$ & 18%, $L_u^x/D = 0.53$) are significant in that they extend the Reynolds number–turbulence intensity envelope for wind-tunnel studies. The results indicated that high-intensity turbulence acted to promote transcritical flow. This effect has been anticipated, but these results are the first clear indication in a wind-tunnel experiment. However, the values of sectional C_l' and spectral bandwidth parameter B obtained in the experiments were comparatively high, suggesting that the results cannot be used directly in the prediction of full-scale structural response to vortex shedding.

Comparison with results measured on full-scale structures at higher Reynolds numbers, similar turbulence intensities, but higher turbulence-length-scale ratios suggest that the turbulence length scale is also an important parameter for determining fluctuating lift at high Reynolds numbers. A plot of sectional values of C_l' obtained at the high end of the Reynolds number range in this experiment ($Re \approx 5 \times 10^5$) against the turbulence parameter Ta proposed by Vickery followed an extrapolation of the trend of values obtained from full-scale investigations. This supports Vickery's suggestion that coefficients of vortex-induced lift in the transcritical regime may be increasing functions of this parameter.

The first author would like to acknowledge financial support provided in the early stages of this research in the form of a Monash Graduate Scholarship. Additional financial support was provided by the Australian Research Council.

REFERENCES

ACHENBACH, E. & HEINECKE, E. 1981 On vortex shedding from smooth and rough cylinders in the range of Reynolds numbers from 6×10^3 to 5×10^6. *J. Fluid Mech.* **109**, 239–251.

BATCHELOR, G. K. 1953 *The Theory of Homogeneous Turbulence*. Cambridge University Press.

BATHAM, J. P. 1973 Pressure distributions on circular cylinders at critical Reynolds numbers. *J. Fluid Mech.* **57**, 209–228.

BEARMAN, P. W. 1969 On vortex shedding around a circular cylinder in the critical Reynolds number regime. *J. Fluid Mech.* **37**, 577–585.

BLACKBURN, H. M. 1992 Lift on an oscillating cylinder in smooth and turbulent flows. PhD thesis, Monash University, Melbourne.

BLACKBURN, H. M. 1994 Effect of blockage on spanwise correlation in a circular cylinder wake. *Exps. Fluids* **18**, 134–136.

BLACKBURN, H. M. & MELBOURNE, W. H. 1992 Lift on an oscillating cylinder in smooth and turbulent flow. *J. Wind Engng Ind. Aero.* **41**, 79–90.

BRUUN, H. H. & DAVIES P. O. A. L. 1975 An experimental investigation of the unsteady pressure forces on a circular cylinder in a turbulent cross flow. *J. Sound Vib.* **40**, 535–559.

CHEUNG, J. C. K. 1983 Effect of turbulence on the aerodynamics and response of a circular structure in air flow. PhD thesis, Monash University, Melbourne.

CHEUNG, J. C. K. & MELBOURNE, W. H. 1983 Turbulence effects on some aerodynamic parameters of a circular cylinder at supercritical Reynolds numbers. *J. Wind Engng Ind. Aero.* **14**, 399–410.

FAGE, A. & WARSAP, J. H. 1930 *ARC R&M 1283* (also § 191, *Modern Developments in Fluid Dynamics* ed. S. Goldstein, Clarendon Press 1938, republished by Dover, 1965).

FARELL, C. & BLESSMAN, J. 1983 On critical flow around smooth circular cylinders. *J. Fluid Mech.* **136**, 375–391.

FOX, T. A. & WEST, G. S. 1990 On the use of end plates with circular cylinders. *Exps. Fluids* **9**, 237–239.

GERRARD, J. H. 1961 An experimental investigation of the oscillating lift and drag of a circular cylinder shedding turbulent vortices. *J. Fluid Mech.* **11**, 244–256.

GÜVEN, O., PATEL, V. C. & FARELL, C. 1977 A model for high-Reynolds-number flow past rough-walled cylinders. *Trans. ASME* I: *J. Fluids Engng* **99**, 486–493.

HOWELL, J. K. & NOVAK, M. 1979 Vortex shedding from circular cylinders in turbulent flow. In *Proc. 5th Intl Conf. Wind Effects Build. & Struct. Colorado, July* (ed. J. E. Cermak), pp. 619–629. Pergamon.

JAMES, W. D, PARIS, S. W. & MALCOLM, G. N. 1980 Study of viscous crossflow effects on circular cylinders at high Reynolds numbers. *AIAA J.* **18**, 1066–1072.

JONES, S. W., CINCOTTA, J. J. & WALKER, R. W. 1969 Aerodynamic forces on a stationary and oscillating circular cylinder at high Reynolds numbers. *NASA TR* R–300.

KEEFE, R. T. 1962 Investigation of the fluctuating forces acting on a stationary circular cylinder in a subsonic stream and of the associated sound field. *J. Acoust. Soc. Am.* **34**, 1711–1714.

NORBERG, C. & SUNDÉN, B. 1987 Turbulence and Reynolds number effects on the flow and fluid forces on a single cylinder in cross flow. *J. Fluids Struct.* **1**, 337–357.

PRESS, W. H., FLANNERY, B. P., TEUKOLSKY, S. A. & VETTERLING, W. T. 1992 *Numerical Recipes in C: The Art of Scientific Computing*, 2nd edn. Cambridge University Press.

RICHTER, A. & NAUDASCHER, E. 1976 Fluctuating forces on a rigid cylinder in confined flow. *J. Fluid Mech.* **78**, 561–576.

ROSHKO, A. 1961 Experiments on the flow past a circular cylinder at very high Reynolds number. *J. Fluid Mech.* **10**, 345–356.

RUSCHEWEYH, H. & HIRSCH, G. 1975 Full scale measurements of the dynamic response of tower shaped structures. In *Proc. 4th Int. Conf. Wind Effects Build. & Struct. Heathrow*, pp. 133–142.

SANADA, S. & NAKAMURA, O. 1983 Full-scale measurements of wind forces acting on a 200 m concrete chimney. *Kajima Institute of Construction Technology Report. Tokyo.*

SANADA, S., SUZUKI, M. & MATSUMOTO, H. 1992 Full-scale measurements of wind forces acting on a 200 m concrete chimney, and the chimney's response. *J. Wind Engng Ind. Aero.* **43**, 2165–2176.

SCHEWE, G. 1983 On the force fluctuations acting on a circular cylinder in crossflow from subcritical up to transcritical Reynolds numbers. *J. Fluid Mech.* **133**, 265–285.

SHIH, W. C. L., WANG, C., COLES, D. & ROSHKO, A. 1993 Experiments on flow past rough circular cylinders at large Reynolds numbers. *J. Wind Engng Ind. Aero.* **49**, 351–368.

SO, R. M. & SAVKAR, S. D. 1981 Buffeting forces on rigid circular cylinders in cross flows. *J. Fluid Mech.* **105**, 397–425.

STANSBY, P. K. 1974 The effects of end plates on the base pressure coefficient of a circular cylinder. *Aero. J.*, January, 36–37.

SURRY, D. 1972 Some effects of intense turbulence on the aerodynamics of a circular cylinder at subcritical Reynolds number. *J. Sound Vib.* **52**, 543–563.

SZEPESSY, S. & BEARMAN, P. W. 1992 Aspect ratio and end plate effects on vortex shedding from a circular cylinder. *J. Fluid Mech.* **234**, 191–217.

UBEROI, M. S. 1956 Effect of wind-tunnel contraction on free-stream turbulence. *J. Aero. Sci.* **23**, 754–764.

VICKERY, B. J. 1991 Progress and problems in the prediction of the response of prototype structures to vortex-induced vibration. *J. Wind Engng Ind. Aero.* **33**, 181-196.

VICKERY, B. J. & CLARK, A. W. 1972 Lift or across-wind response of tapered stacks. *ASCE J. Struct. Div.* ST1 **98**, 1–20.

VICKERY, B. J. & DALY, A. 1984 Wind tunnel modelling as a means of predicting the response of chimneys to vortex shedding. *Engng Struct.* **6**, 364–368.

WEST, G. S. & APELT, C. J. 1982 The effects of tunnel blockage and aspect ratio on the mean flow past a circular cylinder with Reynolds numbers between 10^4 and 10^5. *J. Fluid Mech.* **114**, 361–377.

WEST, G. S. & APELT, C. J. 1993 Measurements of fluctuating pressures and forces on a circular cylinder in the Reynolds number range 10^4 to 2.5×10^5. *J. Fluids Struct.* **7**, 227–244.

ZDRAVKOVICH, M. M. 1991 Conceptual overview of laminar and turbulent flows past smooth and rough circular cylinders. *J. Wind Engng Ind. Aero.* **33**, 53–62.